Electronic Supplementary Material (ESI) for CrystEngComm.

Supplementary material

Growth Kinetics of Curcumin Form I

Claire Heffernan[1,†], *Rodrigo Soto*[1,†,*], *Benjamin K. Hodnett*[1], *Åke C. Rasmuson*[1,2]

[1]*Synthesis and Solid State Pharmaceutical Centre (SSPC), Bernal Institute, Department of Chemical and Environmental Science, University of Limerick. Limerick V94 T9PX, Ireland.*

[2]*Department of Chemical Engineering and Technology, KTH Royal Institute of Technology, SE-100 44 Stockholm, Sweden*

[†] These authors contributed equally.

**Corresponding author email:* rodrigo.soto@ul.ie

S1. HPLC Analysis of Seed Material for purity determination

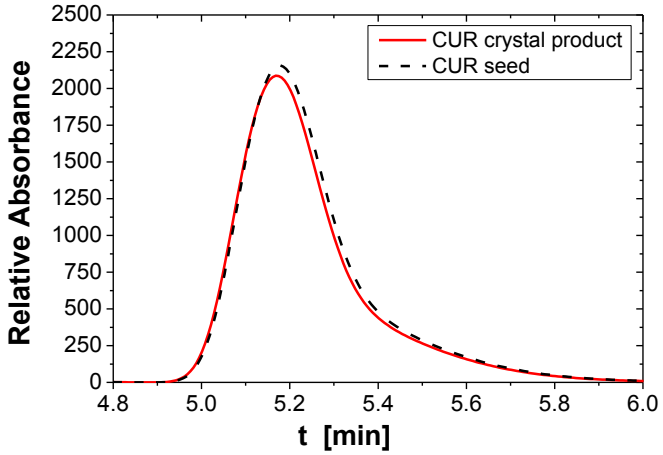

Figure S1. HPLC Chromatogram of the CUR Seeds and CUR crystal product. One peak is shown at retention time of ~ 5.2 min indicating pure CUR seed and CUR crystal product.

S2. Further experimental and data analysis details

S2.1. Materials and instrumentation used

Commercially available crude CUR of >75 % nominal purity (HPLC, area %) was obtained from Merck, comprising of < 20% DMC and < 5% BDMC. Propan-2-ol (99.9 %GC, Merck) was purchased from VWR. An pure reference standard of CUR (100% purity, verified via HPLC) was separated and purified from crude CUR (Merck) by a number of recrystallizations in propan-2-ol. The method used for the recrystallizations is published in previously reported work.[1] The solubility of pure solid CUR in propan-2-ol has been determined by the gravimetric and analytical method previously reported[1,2] and are used here for calculation of the prevailing supersaturation (c/c^*).

The HPLC system and analytical method used in this study to analyse the CUR samples are reported in previously published work.[3] A PANalytical Empyrean diffractometer system using Bragg−Brentano geometry and an incident beam of Cu K-alpha radiation (λ = 1.5418 Å) was used to record the X-ray diffraction patterns of CUR. Room temperature scans were operated on a spinning silicon sample holder using a step size of 0.013 °2θ and a step time of 32 s. Morphology G3 particle size and shape analyser (Malvern instruments) was used to determine the HS Circularity, CE Diameter (µm) and crystal size distribution (CSD) of the CUR seed particles and CUR crystal product. Images of the CUR particles are also obtained using this instrument at optic 5x magnification. Hitachi SU-70 Field Emission SEM was used to observe the CUR specimens in their native state; conductive coatings were avoided. To minimize specimen charging a low primary electron beam energy (1 keV) was used for all image acquisitions. A Zeiss MCS651 spectrometer fitted with a Hellma 661.812 Attenuated Total Reflection (ATR) UV-Vis fiber optic immersion probe (Clairet Scientific, Northampton, UK) was used to measure the changes in the solution concentration of CUR by measuring the absorbance of CUR at a scan time of every 1 min. The spectral wavelength used was 199 – 600 nm using Aspect Plus software since the curcuminoids absorb in the UV – Visible wavelength at 425 nm.

S.2.2. Further details on the data analysis (UV-Vis+PCA and non-linear regression)

An example of typical UV-Vis spectra obtained during the runs is plotted in Figure S2, where the maximum absorbance is observed at approximately 440 nm. In most of the cases, the first principal component was able to explain more than 95% of the system variance, but in some cases, also the second principal component was needed to achieve an acceptable and reliable description of the system variance. The final scores were used to correlate experimental data to the liquid concentration of CUR at any time by means of a calibration free method.[4] Such methodology is for the first time shown to be applicable to track the concentration of curcumin solutions.

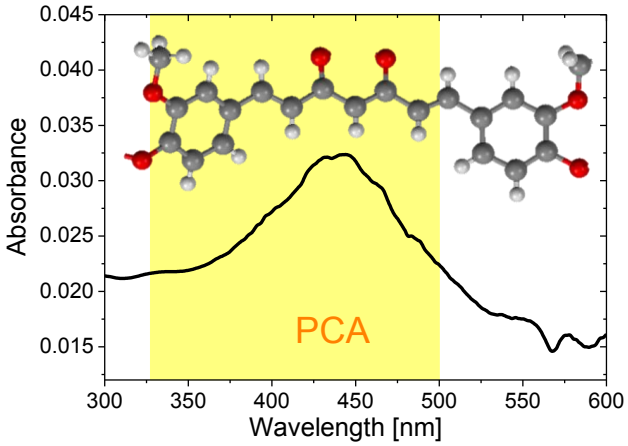

Figure S2. Example of typical UV-Vis spectrum data for the system CUR-propan-2-ol in the range 300-600 nm. Yellow area highlights the region wherein PCA was applied.

Non-linear regression was performed in a created MATLAB script by the minimization of the squared sum of residuals (*SSR*) between the experimentally determined driving forces and those calculated from the solution of the corresponding differential equation (e.g. manuscript Eq.1). The MATLAB functions *ode23tb* and *lsqcurvefit* were used to solve the differential equations and to perform the optimization, respectively. The function *nlparci* was used to account for the errors associated with the estimation of parameters within a 95% confidence interval. The correlation coefficients between the estimates were calculated through the covariance matrix. The initial values of the estimates were altered by several orders of magnitude to validate that a global minimum has been reached.

S3. Regression Analysis and compilation of data for comparison

Figure S3, represents comparison examples of the fitting provided by each model. Both empirical and mechanistic models fitted experimental data in a reasonably good fashion. By simple visual inspection, the B+S model was the worst fitting observed.

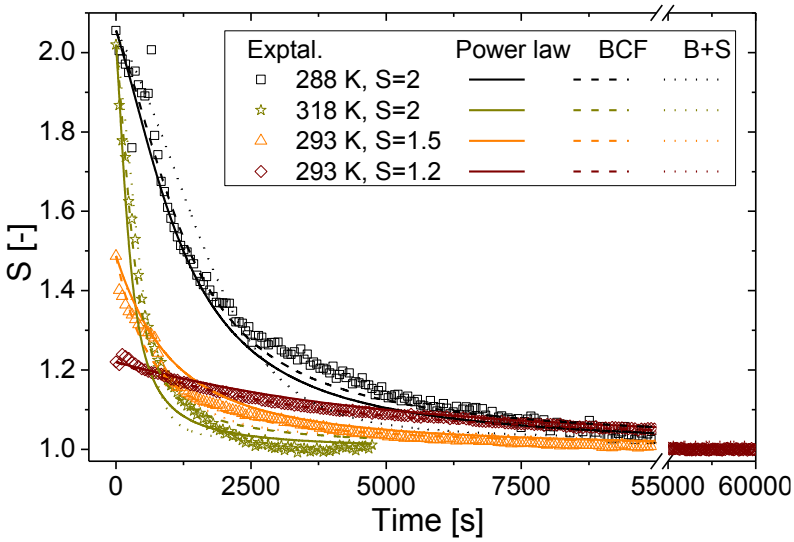

Figure S3. Examples of the fitting to experimental data provided by power law, BCF and B+S models at different experimental conditions.

Table S1. Comparison of growth kinetic constants (k_g) reported for different systems

T_{cryst} [K]	k_g [m/s]	Crystal growth system
298	$9.42 \cdot 10^{-8}$	This work
298	$1.02 \cdot 10^{-4}$	Salicylic acid in methanol [5]
298	$5.01 \cdot 10^{-5}$	Salicylic acid in acetone [5]
298	$3.09 \cdot 10^{-5}$	Salicylic acid in acetonitrile [5]
298	$9.67 \cdot 10^{-5}$	Salicylic acid in Ethyl acetate [5]
298	$3.33 \cdot 10^{-6}$	Salicylamide in methanol [6]
298	$6.58 \cdot 10^{-5}$	Salicylamide in acetone [6]
298	$5.02 \cdot 10^{-5}$	Salicylamide in acetonitrile [6]
298	$2.91 \cdot 10^{-5}$	Salicylamide in ethyl acetate [6]
298	$2.01 \cdot 10^{-6}$	Piracetam FII in ethanol [7]
298	$7.23 \cdot 10^{-7}$	Piracetam FII in isopropanol [7]
298	$1.02 \cdot 10^{-6}$	Piracetam FIII in ethanol [7]
298	$3.78 \cdot 10^{-7}$	Piracetam FIII in isopropanol [7]
303	$3.51 \cdot 10^{-11}$	Iron fluoride trihydrate [8]
289	$5.90 \cdot 10^{-5}$	Paracetamol in acetone [9]

Table S2. Examples of previously reported values of γ_{sl} in crystal growth studies

Crystal growth system	**γ_{sl} [mJ/m^2]**
This work	2.65
Salicylic acid in Ethyl acetate[a]	0.58
Salicylic acid in acetonitrile[a]	0.65
Salicylic acid in acetone[a]	0.79
Salicylic acid in methanol[a]	1.10
Salicylamide acid in Ethyl acetate[b]	0.81
Salicylamide acid in acetonitrile[b]	0.54
Salicylamide acid in acetone[b]	0.49
Salicylamide acid in methanol[b]	0.41
Piracetam FII in ethanol[c]	1.12
Piracetam FIII in ethanol[c]	1.75
Piracetam FII in isopropanol[c]	1.12
Piracetam FIII in isopropanol[c]	2.08
Paracetamol in water-toluene-acetone mixtures[d]	1.2-2.3
Nucleation of pure CUR Form I[e]	4.45

[a] From L. Jia et al. (2017) [5]. [b] From A. Lynch et al (2018)[6]. [c]From R. Soto and Å. C. Rasmuson (2019)[7]. [d] From R.A. Granberg and Å. C. Rasmuson (2005)[10]. [e] From C. Heffernan et al. (2018)[11].

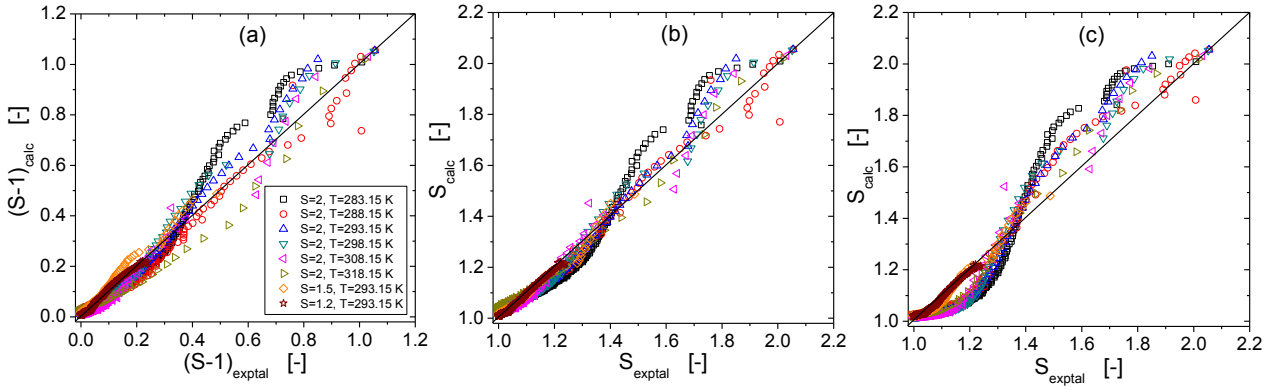

Figure S4. Parity plots corresponding to the fitting of: **(a)** Power law equation, **(b)** BCF model and, **(c)** B+S model.

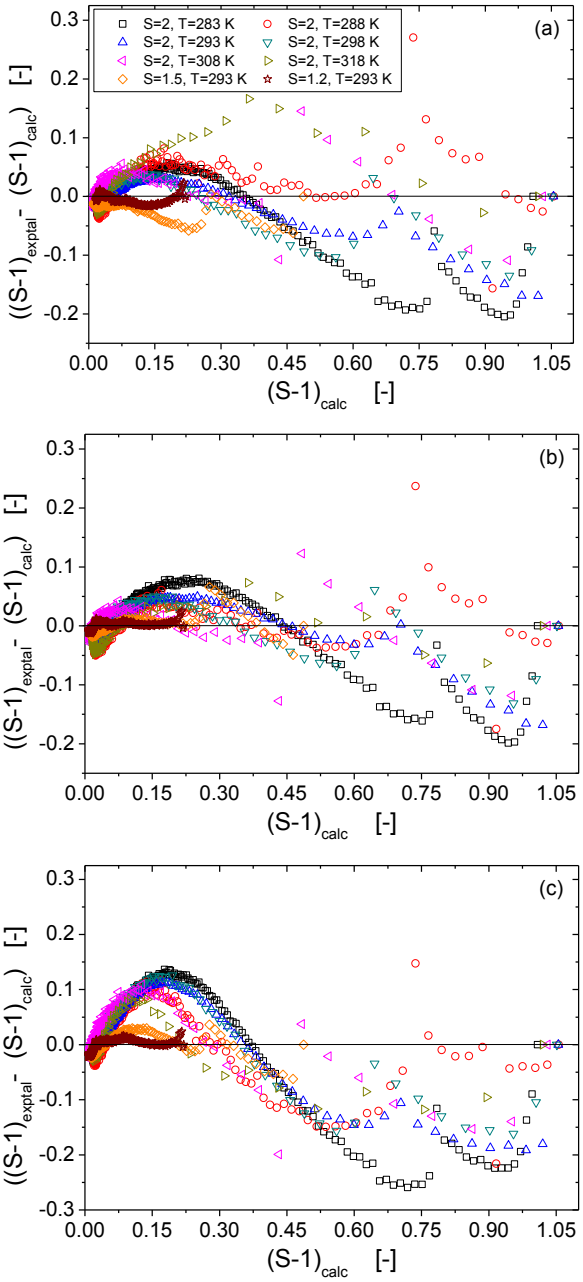

Figure S5. Residuals plot for the modelling of: (a) full power law equation, (b) BCF, and (c) B+S.

Residuals of power law and BCF models showed some heteroscedasticity (increasing variance with magnitude) whereas B+S model residuals showed both heteroscedasticity and drift. The parity plots of the power law equation and the BCF model revealed that both models fitted the experimental data quite well at low supersaturations. Although the B+S model also provided an acceptable fitting (refer to the parity plot and residuals analysis), a more evident systematic behaviour is observed for most of the runs, i.e. it tends to underestimate the experimental driving forces at high supersaturations and to overestimate them at low supersaturations.

References

1 M. Ukrainczyk, B. K. Hodnett and Å. C. Rasmuson, *Org. Process Res. Dev*, 2016, **20**, 1593–1602.

2 J. Liu, M. Svärd, P. Hippen and Å. C. Rasmuson, *J. Pharm. Sci.*, 2015, **104**, 2183–2189.

3 C. Heffernan, M. Ukrainczyk, R. K. Gamidi, B. K. Hodnett and Å. C. Rasmuson, *Org. Process Res. Dev.*, 2017, **21**, 821–826.

4 J. Cornel and M. Mazzotti, *Ind. Eng. Chem. Res.*, 2009, **48**, 10740–10745.

5 L. Jia, M. Svärd and Å. C. Rasmuson, *Cryst. Growth Des.*, 2017, **17**, 2964–2974.

6 A. Lynch, L. Jia, M. Svärd, Å. C. Rasmuson, *Cryst. Growth Des.*, 2018, **18**, 7305-7315.

7 R. Soto and Å. C. Rasmuson, *Cryst. Growth Des.*, 2019, **19**, 8, 4273-4286.

8 K. M. Forsberg and Å. C. Rasmuson, *J. Cryst. Growth*, 2006, **296**, 213–220.

9 R. A. Granberg, D. G. Bloch and Å. C. Rasmuson, *J. Cryst. Growth*, 1999, **198**–**199**, 1287–1293.

10 R. A. Granberg and Å. C. Rasmuson, *AIChE J.*, 2005, **51**, 2441–2456.

11 C. Heffernan, M. Ukrainczyk, J. Zeglinski, B. K. Hodnett and Å. C. Rasmuson, *Cryst. Growth Des.*, 2018, **18**, 4715–4723.